Improved Design of Sliding-Mode Controllers Based on the Requirements of MPPT Techniques

Daniel González Montoya, *Student Member, IEEE*, Carlos Andrés Ramos-Paja, *Senior Member, IEEE*, and Roberto Giral, *Senior Member, IEEE*

***Abstract*—In many grid-connected applications, a dc/dc switching converter is usually connected between the PV modules and the inverter. This paper presents an improved procedure to design a sliding controller for the PV system, which drives the PV voltage to follow a reference provided by an external MPPT algorithm and mitigates the perturbations caused by the irradiance changes and oscillations in the bulk voltage. By considering that the switching surface is the linear combination of the input capacitor current and the PV voltage error, the proposed design exhibits advantages in comparison with existing solutions that rely in the linearization of inner current loop dynamics. The proposed integral procedure, by taking also into account the effects in the closed-loop system dynamics of a reference filter, ensures a stable sliding regime in all the desired operation range of the system, while the settling time and overshoot of the PV voltage required by an MPPT algorithm are provided. Differently from a previous similar but less rigorous approach, the switching function and reference filter parameters are obtained by numerically solving a set of nonlinear equations. Simulations and experiments were used to demonstrate the efficiency of the proposed solution in presence of environmental and load perturbations.**

***Index Terms*—DC-DC power converter, maximum power point tracker, Nonlinear control systems, photovoltaic system, sliding mode control.**

I. Introduction

PHOTOVOLTAIC (PV) systems are a suitable option to produce clean electrical energy since they can be dimensioned for a wide range of power ratings in both stand-alone and grid-connected applications [1], [2]. A typical PV system is composed by a PV array, a dc/dc converter to transform the power provided by the PV source, and an inverter, as depicted in Fig. 1. The PV array is characterized by a nonlinear behavior that changes significantly with the operating conditions, e.g., irradiance level, shades, temperature, among others, which makes difficult to predict the voltage and current to guarantee the maximum power production [3]. The operation point in which the PV array provides its maximum power is named maximum power point (MPP) [4], [5]. Then, the main objective of the control strategy in a PV system is to ensure the system operation around its MPP (maximum power point tracking—MPPT) in whichever load and environmental conditions [3]–[6]. In the literature, the most commonly used MPPT solutions are the incremental conductance and the perturb and observe (P&O) [7], where the P&O is widely adopted due to its simple implementation and tracking efficiency [4], [8].

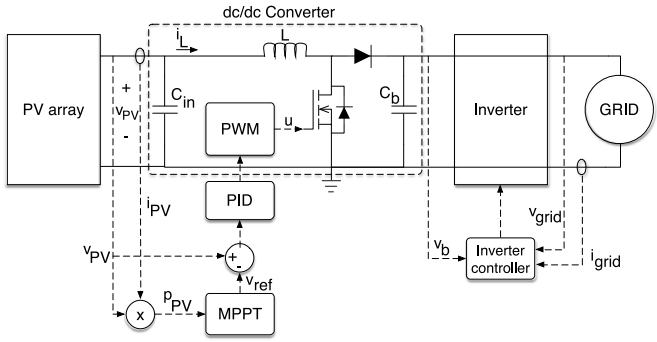

Fig. 1. PV system scheme based on classical PID controller.

The connection between the dc/dc converter and the inverter causes voltage oscillations since the power delivered by the PV panel is dc and the power injected by the inverter is ac [9], [10]. If such oscillations are not well mitigated, the PV power delivered to the grid may be affected, also making difficult the tracking of the MPP by the MPPT algorithm [4]. To face this problem, an electrolytic capacitor is connected between the dc/dc converter and the inverter, as illustrated in Fig. 1, but such a solution decreases the reliability of the system [11].

Many solutions have been proposed to mitigate such oscillations [4], [9]. Usually, the first alternative is to design a linear controller (PI, PID, or lead-lag) to guarantee a satisfactory tracking of the voltage reference generated dc/dc by the MPPT algorithm (see Fig. 1), and at the same time to mitigate the perturbations generated by the load and by the irradiance variations [12]. The main problem associated to this kind of controllers concerns the requirement of linearizing the model of the PV system around a given operating point, which does not ensure the same performances in all the PV operation range.

Other types of controllers have been proposed in the literature to improve the behavior of the PV system accounting for changes on the operating point. Some of those controllers are based on adaptive laws [3], energy balance [13], and sliding-mode theory. In particular, the sliding-mode approach offers stability and

Manuscript received June 4, 2014; revised December 4, 2014; accepted January 20, 2015. Date of publication January 28, 2015; date of current version September 21, 2015. This work was supported by the Universidad Nacional de Colombia under the Project RECONF-PV-25633, by the scholarship 2012-567 from Departamento Administrativo de Ciencia, Tecnología e Innovación-COLCIENCIAS, Colombia, by the Universitat Rovira i Virgili, and by the Spanish Ministerio de Economía y Competitividad under Project CSD2009-00046 and Project TEC2012-30952. Recommended for publication by Associate Editor G. Escobar.

D. G. Montoya and C. A. Ramos-Paja are with the Facultad de Minas, Universidad Nacional de Colombia, Medellin, 050034 Colombia (e-mail: dgonzalm@unal.edu.co; caramosp@unal.edu.co).

R. Giral is with the Departament d'Enginyeria Electronica, Electrica i Automatica, Universitat Rovira i Virgili, 43007 Tarragona, Spain (e-mail: roberto.giral@urv.cat).

Color versions of one or more of the figures in this paper are available online at http://ieeexplore.ieee.org.

Digital Object Identifier 10.1109/TPEL.2015.2397831

robustness against parameters, input and load uncertainties, which are common in PV systems. Moreover, sliding-mode controllers (SMC) are simpler to implement in comparison with other types of nonlinear controllers [14]. Therefore, some solutions based on SMC have been proposed to provide a good performance in the mitigation of the load voltage oscillations and to ensure the tracking of the reference provided by the MPPT algorithm [14]–[18]. However, in general, these solutions do not guarantee the existence of the sliding mode in all the operation range. Moreover, the reported design of the SMC parameters is not necessarily related with the requirements of the MPPT algorithm, hence it is difficult to ensure the desired behavior of the complete PV system, e.g., an accurate settling time of the PV voltage is required to ensure the stability of a P&O algorithm at any operation condition [4], [19].

This paper proposes an integral procedure to design an SMC accounting for all the elements required to ensure the desired operation of the PV system, i.e., a stable SMC to track the reference provided by an MPPT algorithm in presence of load and environmental perturbations. Such a design procedure is aimed at providing the settling time and overshoot that ensures a stable operation of the MPPT algorithm at any operation condition. The procedure overcomes the defects of the previous approach reported in [20], in which the design of an inner current capacitor loop is followed by the designs of a cascaded voltage PI controller and a first-order low-pass filter that limits the voltage reference derivative.

This paper is organized as follows: Section II presents the review of some solutions based on SMC, where the disadvantages inherent to each solution are put in evidence. Based on such reviews, a new design procedure for SMC in PV systems is introduced. Section III presents the analysis of the SMC to ensure the PV voltage stability in the operation range. Then, Section IV provides the design and implementation procedure for the SMC, based on the requirements of a P&O algorithm, to track the MPP in presence of perturbations. Section V illustrates the SMC design accounting for realistic conditions, presenting also simulations results. Experimental validations together with many details on the controller implementation aimed at helping to reproduce the results are reported in Section VI, while Section VII closes this paper with the conclusions.

II. Background of the Proposed Design Procedure

The control structure presented in Fig. 1 is commonly used to regulate the PV voltage to follow the reference given by the MPPT algorithm, and at the same time, to mitigate both the perturbations propagated from the load and those generated by changes on the environmental conditions [12]. The PID controller is designed using a linear model of the PV system around a specific operating point, e.g., the MPP at the lowest irradiance level [4]. Thus, to guarantee the same performance in all the operation in the range, it is necessary to design more robust controllers that do not depend on linearized models only.

The solution proposed in this paper is based on two previous works published in [15] and [20], which apply the sliding-mode technique to regulate the PV voltage and to mitigate the low-frequency voltage oscillations caused at the bulk capacitor C_b

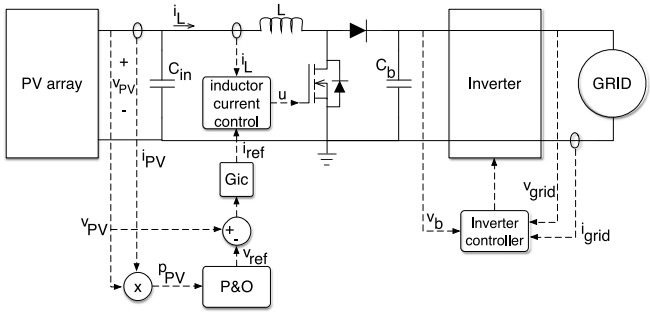

Fig. 2. PV system scheme based on the inductor current control.

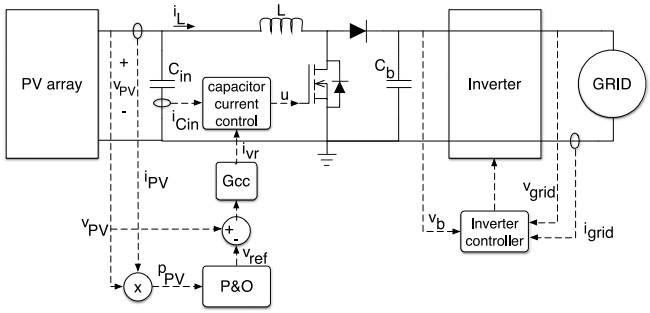

Fig. 3. System scheme based on input capacitor current control.

by the inverter operation [12], [21]. The first implementation, given in [15] and presented in Fig. 2, is based on the regulation of the average input current of the boost converter by means of the inductor current control. The voltage and current of the PV array are provided to a P&O algorithm, which defines the reference to the voltage controller G_{ic}. Such a linear controller imposes the reference $i_{\rm ref}$ to the SMC based on the switching function Ψ_{i_L} and surface Φ_{i_L} given in

$$\Psi_{i_L} = i_L - i_{\rm ref} \quad \wedge \quad \Phi_{i_L} = \{\Psi_{i_L} = 0\}. \tag{1}$$

The design of the G_{ic} controller is based on the linearized model given in (2), which considers the inductor current controlled by the SMC as a current source. Such a condition generates the main problem of this first approach: The transfer function $G_{v_{\rm PV}/i_{\rm ref}}$ is based on the parameter $R_{\rm MPP}$ that models the impedance of the PV panel. Therefore, (2) must be evaluated in some operating point in order to obtain a transfer function suitable for design the controller G_{ic}. However, when the PV array experiments changes in the irradiance or in the temperature, the value of $R_{\rm MPP}$ changes, which makes the controller design based on the evaluated (2) not suitable to ensure a consistent performance in all the PV system operation range

$$G_{v_{\rm PV}/i_{\rm ref}} = \frac{V_{\rm PV}(s)}{I_{\rm ref}(s)} = -\frac{R_{\rm MPP}}{1 + R_{\rm MPP} \cdot C_{\rm in} \cdot s}. \tag{2}$$

The second implementation, given in [20] and presented in Fig. 3, is based on the regulation of the input capacitance current $i_{C_{\rm in}}$. In this approach, sensing the capacitor current is simpler than sensing the inductor current because $i_{C_{\rm in}}$ exhibits a zero dc component and the sensor is connected to the ground.

Similar to the previous solution, a P&O algorithm generates the reference of the voltage controller G_{cc}, which produces the reference i_{vr} of the input capacitor current SMC based on the switching function $\Psi_{i_{C_{\rm in}}}$ and surface $\Phi_{i_{C_{\rm in}}}$ given in

$$\Psi_{i_{C_{\rm in}}} = -i_{C_{\rm in}} - i_{vr} \quad \wedge \quad \Phi_{i_{C_{\rm in}}} = \left\{ \Psi_{i_{C_{\rm in}}} = 0 \right\}. \tag{3}$$

That surface imposes changes in the capacitor current $i_{C_{\rm in}}$ to mitigate both the perturbations present in the bulk capacitor voltage v_b and the perturbations caused by the irradiance changes. The controller G_{cc} design is based on the linearized model given in (4). This control approach presents an improvement with respect to the previous work because transfer function (4) does not depend on any PV panel parameter, hence the designed controller must provide the same behavior regardless the operation conditions [20]

$$\frac{V_{\rm PV}(s)}{I_{C_{\rm in_{ref}}}(s)} = -\frac{1}{C_{\rm in} \cdot s}. \tag{4}$$

However, the switching function in (3) can be rewritten as in (5) where K_p and K_i are the proportional and integral parameters of the PI controller. Then, the main problem of the design process in [20] concerts the adoption of three strong simplifications that makes impossible to guarantee the system performance in all the operation range: first, considering the SMC as a current source to design K_p and K_i exclusively based on (4). However, as reported in (5), the sliding surface depends on K_p and K_i, hence the sliding-mode analysis must account K_p and K_i values to ensure stability

$$\Psi_{i_{C_{\rm in}}} = -i_{C_{\rm in}} - K_p \cdot (v_{\rm PV} - v_{\rm ref}) - K_i \cdot \int (v_{\rm PV} - v_{\rm ref})\, dt. \tag{5}$$

The second simplification is to consider the PV voltage constant even in presence of changes in both the irradiance and the capacitor current, which is not true, hence the stability analysis with such assumption is not general. The third simplification is to assume that a prefilter inserted between the reference and the controller that does not modify the settling time and overshoot of the PV voltage, which is not true since such a filter changes the reference waveform provided to the SMC. Moreover, the controller G_{cc} design requires a reduction of the system bandwidth, which is usually close to $1/5$ of the switching frequency, to guarantee a good performance in all operation range [19]. However, due to the changes in the switching frequency caused by the SMC implementation based on hysteresis comparators, such a condition is not granted.

The previous disadvantages of the design procedures reported in [15] and [20] severely affect the performance of the PV system: First, the stability condition of the P&O algorithm imposes that the perturbation period must be longer than the settling time of the PV voltage as demonstrated in [4] and [19]. The design procedures in [15] and [20] are not able to guarantee such a condition. Second, it is desirable to ensure a null overshot in the PV voltage to avoid power losses due to oscillations around the MPP, however the procedures reported in [15] and [20] do not ensure such a performance. Therefore, such solutions do not ensure a correct tracking of the MPP, or even system stability, in the complete operation range.

III. Analysis of the Sliding Controller

Based on the previous section, it is required to design a process for the SMC that ensures the system stability, the desired settling time, and null overshoot. Therefore, such a design process must to take into account all the elements in the control loops, e.g., requirements of the MPPT algorithm, SMC, filters, etc.

A good alternative to define the behavior of the PV voltage $v_{\rm PV}$ is to include both the error with respect to the reference and the voltage derivative into the switching function, where the voltage derivative can be acquired by measuring the input capacitor current $i_{C_{\rm in}}$. The main advantage of such a switching function concerns the regulation of the PV voltage without additional controllers based on linearized models. Therefore, this paper is based on the switching function Ψ and surface Φ given in (6), which enable to analyze the stability of the PV voltage in presence of load, environment, or reference changes

$$\Psi = (v_{\rm PV} - v_{\rm ref}) \cdot K_1 + i_{C_{\rm in}} \cdot K_2 \quad \wedge \quad \Phi = \{\Psi = 0\}. \tag{6}$$

It must be pointed out that such a switching function Ψ is similar to the one adopted in [20], i.e., equivalent switching function (5). However, this paper is focused in providing a new analysis and design procedure for the control system, without including any of the simplifications adopted in [20], to guarantee a stable behavior of the SMC and a correct tracking of the MPP.

The scheme presented in Fig. 4(a) is used to implement the switching function Ψ, where the voltage reference $v_{\rm ref}$ is provided by a P&O controller. The dynamic behavior of the dc/dc converter is modeled by (7) and (8), where $i_{\rm PV}$ and v_b represent the PV current and the bulk voltage, respectively, while the manipulated variable u corresponds to the activation signal of the semiconductor switches

$$i_{C_{\rm in}} = C_{\rm in} \cdot \frac{dv_{\rm PV}}{dt} = i_{\rm PV} - i_L \tag{7}$$

$$v_L = L \cdot \frac{di_L}{dt} = v_{\rm PV} - v_b \cdot (1-u). \tag{8}$$

The PV current can be modeled by the simplified single-diode model (9) [20], [22], where $i_{\rm SC}$ represents the short-circuit current, I_R is the diode saturation current, and α represents the thermal voltage that depends on the array temperature [20]. The parameters of this model can be calculated from the operation condition and datasheet values as described in [22], where the short-circuit current is approximately proportional to the irradiance $i_{\rm SC} = K_S \cdot S$ [23]

$$i_{\rm PV} = i_{\rm SC} - I_R \cdot \left(e^{\alpha \cdot v_{\rm PV}} - 1\right). \tag{9}$$

Fig. 4(b) presents the block diagram of the control system including the model of the PV system and the SMC structure, where u is generated using a comparator centered in zero.

The design of a stable SMC requires to fulfill three conditions: Transversality, equivalent control, and reachability [24]. In the following, such conditions are used to develop a design procedure for the control system that ensures the desired performance criteria of the PV voltage.

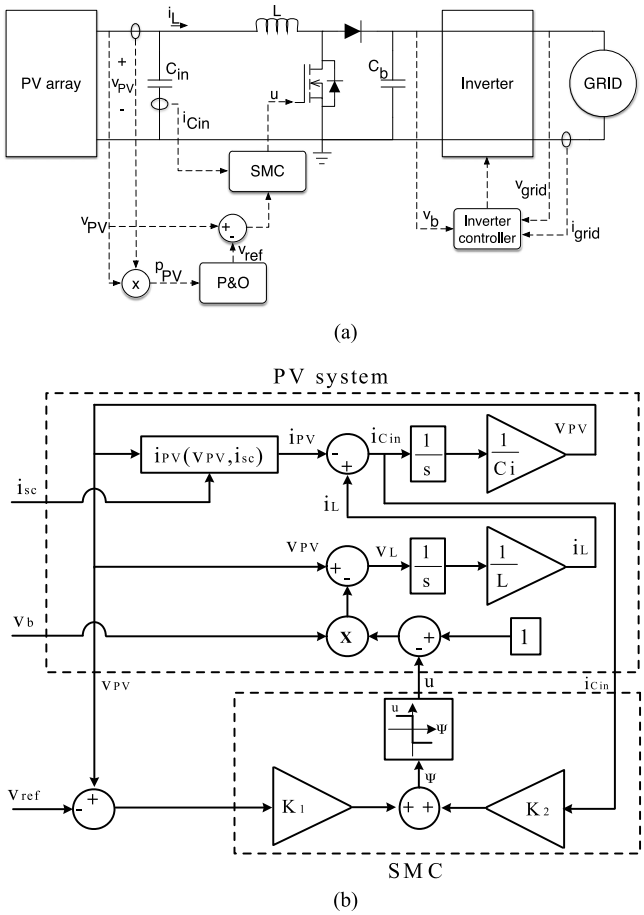

Fig. 4. Sliding mode control based on voltage error and input capacitor current. (a) Circuital scheme. (b) Block diagram.

A. Transversality Condition

The transversality condition (10) guarantees that the manipulated variable u is present in the switching function derivative [14], which is required to modify the system dynamics

$$\frac{d\frac{d\Psi}{dt}}{du} \neq 0. \tag{10}$$

To verify condition (10), the derivative of the function Ψ with respect to the time is obtained in (11) and the derivative of the PV current is given in (12), where $Y = -I_R \cdot \alpha \cdot e^{\alpha \cdot v_{\rm PV}}$

$$\frac{d\Psi}{dt} = K_1 \cdot \left(\frac{dv_{\rm PV}}{dt} - \frac{dv_{\rm ref}}{dt}\right) + K_2 \cdot \left(\frac{di_{\rm PV}}{dt} - \frac{di_L}{dt}\right) \tag{11}$$

$$\frac{di_{\rm PV}}{dt} = \frac{di_{\rm SC}}{dt} + Y \cdot \frac{dv_{\rm PV}}{dt}. \tag{12}$$

Replacing (8) and (12) into (11), the resulting equation is presented

$$\frac{d\Psi}{dt} = \frac{dv_{\rm PV}}{dt} \cdot \left(K_1 + K_2 \cdot \frac{di_{\rm PV}}{dv_{\rm PV}}\right) - K_1 \cdot \frac{dv_{\rm ref}}{dt} + K_2 \cdot \frac{di_{\rm SC}}{dt} - K_2 \cdot \left(\frac{v_{\rm PV} - v_b \cdot (1-u)}{L}\right). \tag{13}$$

The transversality condition is analyzed deriving (13) with respect to u obtaining (14). Then, the transversality condition is fulfilled if the parameter $K_2 \neq 0$ since both v_b and L are positive

$$\frac{d\frac{d\Psi}{dt}}{du} = -\frac{K_2 \cdot v_b}{L} \neq 0. \tag{14}$$

B. Equivalent Control Condition

The next step is to analyze the equivalent control condition, which imposes that the average value $u_{\rm eq}$ of the control variable u must be constrained within the operation range of that control variable [24]. For the dc/dc converter, the correct range is $0 < u_{\rm eq} < 1$. These analyses are illustrated as follows:

$$\frac{d\Psi}{dt} = 0 \rightarrow 0 < u_{\rm eq} < 1. \tag{15}$$

Substituting u by $u_{\rm eq}$ in (13), and inserting such an expression into (15), the following inequality is obtained

$$0 < u_{\rm eq} = \frac{L}{v_b}\left[\left(\frac{K_1}{K_2} + Y\right) \cdot \frac{dv_{\rm PV}}{dt} - \frac{K_1}{K_2} \cdot \frac{dv_{\rm ref}}{dt}\right] + \frac{L}{v_b} \cdot \frac{di_{\rm SC}}{dt} - \frac{v_{\rm PV}}{v_b} + 1 < 1. \tag{16}$$

Moreover, since the analysis considers the system within the surface $\Psi = 0$, (17) is obtained from (6) and (7). Expression (17) describes the sliding-mode dynamics, which can be analyzed in the Laplace domain as given

$$i_{C_{\rm in}} = C_{\rm in} \cdot \frac{dv_{\rm PV}}{dt} = -\frac{K_1}{K_2} \cdot (v_{\rm PV} - v_{\rm ref}) \tag{17}$$

$$\frac{V_{\rm PV}(s)}{V_{\rm ref}(s)} = \frac{1}{\frac{K_2 \cdot C_{\rm in}}{K_1} \cdot s + 1}. \tag{18}$$

Equation (18) shows the existence of an equivalent pole in $-\frac{K_1}{K_2 \cdot C_{\rm in}}$. Therefore, both K_1 and K_2 must to exhibit the same sign to ensure the system stability.

Taking into account that the reference $v_{\rm ref}$ of this SMC is provided by a P&O algorithm as in Fig. 4(a), the reference signal exhibits the following behavior: It remains constant during the perturbation interval T_a; and each T_a seconds, it changes in constant incremental or decremental steps of $\Delta v_{\rm MPPT}$ volts looking for positive changes on the PV power [19]. Then, since relation (18) guarantees that $v_{\rm PV} = v_{\rm ref}$ when the system is in steady state, and taking into account that T_a must be designed longer than the settling of the PV voltage [4], [19], it is concluded that each perturbation of the P&O generates an error of magnitude $\Delta v_{\rm MPPT}$ between the PV voltage and the reference. Such a condition can be formalized as $(v_{\rm PV} - v_{\rm ref}) = \Delta v_{\rm MPPT}$, which could be positive or negative.

Then, replacing (17) into (16), and including the previous consideration, the inequalities (19) and (20) are obtained, as shown at the bottom of the next page.

Inequalities (19) and (20) define the dynamic limits for the derivatives of both the reference and the short-circuit current, i.e., $\frac{dv_{\rm ref}}{dt}$ and $\frac{di_{\rm SC}}{dt}$, respectively. Therefore, the maximum and minimum values of $\frac{dv_{\rm ref}}{dt}$ that must be granted to fulfill the

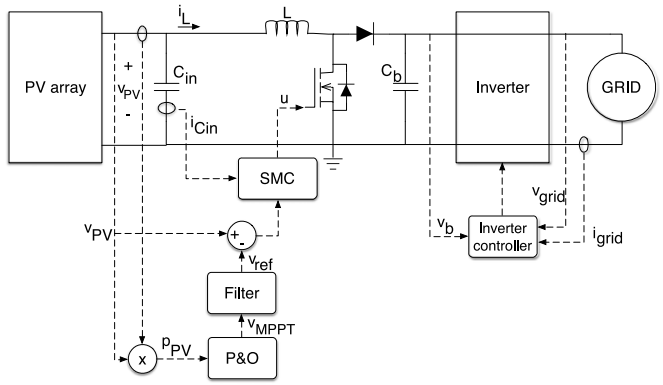

Fig. 5. Complete PV system including the reference filter.

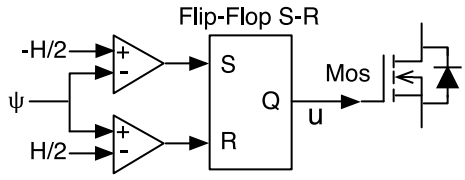

Fig. 6. Implementation scheme of the control action.

equivalent control condition are given by (21) and (22), respectively, as shown at the bottom of the page. Such expressions depend on the maximum irradiance derivative $\frac{dS}{dt}$ and the operating conditions of both the PV array and the dc/dc converter.

The constraints in (21) and (22) put in evidence that step-like waveforms must be avoided in $v_{\rm ref}$, i.e., $\frac{dv_{\rm ref}}{dt} \to \infty$. However, since P&O controllers produce step-like changes on its output signal, it is necessary to introduce a low-pass filter between the P&O controller and the SMC to fulfill (21) and (22). Fig. 5 presents the complete PV system including such a reference filter.

C. Reachability Conditions

The reachability conditions analyze the ability of the system to reach the desired state $\Psi = 0$. The work in [24] demonstrated that a system that fulfills the equivalent control condition also fulfills the reachability conditions. The work also shows that the sign of the transversality condition imposes the value of u for each reachability condition. Due to the implementation constraints, which are discussed in Section IV, the proposed design of the SMC requires a negative value for the parameter K_2. Hence, the transversality condition in (14) is positive, which imposes the reachability conditions (23) and (24) provided that the control action is implemented as $u = 1$ for $\Psi < 0$ and $u = 0$ for $\Psi > 0$ [24]

$$\lim_{\Psi \to 0^-} \left.\frac{d\Psi}{dt}\right|_{u=1} = \left.\frac{d\Psi}{dt}\right|_{u=1,\Psi=0} > 0 \tag{23}$$

$$\lim_{\Psi \to 0^+} \left.\frac{d\Psi}{dt}\right|_{u=0} = \left.\frac{d\Psi}{dt}\right|_{u=0,\Psi=0} < 0. \tag{24}$$

Then, the reachability conditions are calculated by evaluating (13) in (23) and (24), obtaining (25) and (26). By replacing (17) in (25) and (26), the same inequalities given in (19) and (20) as shown on the bottom of the next page are obtained. Therefore, ensuring that $\frac{dv_{\rm ref}}{dt}$ is constrained within the dynamic limits given in (21) and (22) as shown bottom of the page also grants that both reachability conditions are fulfilled, see equation (25) and (26) as shown on the bottom of the next page.

IV. Controller Implementation and Parameters Calculation

This paper uses hysteresis comparators for implementing the SMC, which is a common practice for dc/dc converter applications. Moreover, an hysteresis band H must be added to the sliding surface to limit the switching frequency [14], hence the surface is constrained within $-\frac{H}{2} \leq \Psi \leq \frac{H}{2}$. From such a condition, inequalities (23) and (24) are implemented as in (27), whose electrical scheme is presented in Fig. 6. Its practical realization was performed using a TS555 integrated circuit, which exhibits the same internal structure. The conditions for u in (27) are defined by the positive sign of the transversality condition (14), it requiting a negative value of K_2, which also imposes a negative value to K_1. Adopting positive values for K_1 and K_2 will require additional implementation circuitry

$$\Psi \leq -\frac{H}{2} \to u = 1 \ \wedge \ \Psi \geq \frac{H}{2} \to u = 0. \tag{27}$$

$$\left(\frac{v_{\rm PV} - v_b}{L}\right) + \frac{K_1}{K_2 \cdot C_{\rm in}} \cdot \left(\frac{K_1}{K_2} + Y\right) \cdot \Delta v_{\rm MPPT} < -\frac{K_1}{K_2}\frac{dv_{\rm ref}}{dt} + \frac{di_{\rm SC}}{dt} \tag{19}$$

$$-\frac{K_1}{K_2}\frac{dv_{\rm ref}}{dt} + \frac{di_{\rm SC}}{dt} < \left(\frac{v_{\rm PV}}{L}\right) + \frac{K_1}{K_2 \cdot C_{\rm in}} \cdot \left(\frac{K_1}{K_2} + Y\right) \cdot \Delta v_{\rm MPPT} \tag{20}$$

$$\frac{dv_{\rm ref}}{dt} < \frac{K_2}{K_1} \cdot \left[K_S \cdot \frac{dS}{dt} - \left(\frac{v_{\rm PV} - v_b}{L}\right) - \frac{K_1}{K_2 \cdot C_{\rm in}} \cdot \left(\frac{K_1}{K_2} + Y\right) \cdot \Delta v_{\rm MPPT}\right] \tag{21}$$

$$\frac{dv_{\rm ref}}{dt} > \frac{K_2}{K_1} \cdot \left[K_S \cdot \frac{dS}{dt} - \left(\frac{v_{\rm PV}}{L}\right) - \frac{K_1}{K_2 \cdot C_{\rm in}} \cdot \left(\frac{K_1}{K_2} + Y\right) \cdot \Delta v_{\rm MPPT}\right] \tag{22}$$

A. Switching Frequency Analysis

The SMC implementation based on hysteresis comparators imposes a variable switching frequency $f_{\rm sw}$. Taking into account that the input capacitor and the inductor of the scheme in Fig. 5 form a second-order filter [25] and due to the small-ripple condition of the PV voltage, the magnitude of the current ripples for both the inductor Δi_L and the capacitor $\Delta i_{C_{\rm in}}$ is the same [25], i.e., $\Delta i_{C_{\rm in}} = \Delta i_L$. Then, the switching frequency $f_{\rm sw}$ imposed by the SMC is calculated from the derivative of the inductor current (8) and the duty cycle of the boost converter as in (28). Such an expression can be used to define $\Delta i_{C_{\rm in}}$ in agreement with the practical limitations of the switching frequency imposed by the semiconductors and sensors

$$f_{\rm sw} = \frac{v_{\rm PV} \cdot (v_b - v_{\rm PV})}{\Delta i_{C_{\rm in}} \cdot L \cdot v_b}. \tag{28}$$

B. Calculation of K_2

The sliding-mode behavior, described in (6) and (18), ensures that in steady state $v_{\rm PV} = v_{\rm ref}$, hence the hysteresis $-\frac{H}{2} \leq \Psi \leq \frac{H}{2}$ becomes $-\frac{H}{2} \leq i_{C_{\rm in}} \cdot K_2 \leq \frac{H}{2}$. This expression correlates the hysteresis band H of the sliding surface with the minimum and maximum values of the steady-state current in the input capacitor, which corresponds to the associated current ripple $\Delta i_{C_{\rm in}}$ as given in (29). The magnitude of K_2 can be calculated from

$$\mid K_2 \mid = \frac{H}{\Delta i_{C_{\rm in}}}. \tag{29}$$

Since SMCs are commonly implemented using commercial circuits, e.g., the TS555 and operational amplifiers, H must be chosen according to the operation range of those components. Moreover, $\Delta i_{C_{\rm in}}$ must be designed to guarantee continuous conduction mode and to avoid large ripples in the PV voltage. In addition, as point out in (28), $\Delta i_{C_{\rm in}}$ must be also defined in agreement with the practical limitations of the switching frequency.

C. Design of the Reference Filter

The first step to design the low-pass filter added in Fig. 5 for the voltage reference is to define the filter order. Such a topic was addressed in [20] by using a first-order filter designed as in (30), which avoids overshoots in the reference delivered to the SMC and exhibits a settling time equal to $t_{s,1\rm st} = 3.9 \cdot \tau_f$

$$\frac{v_{\rm ref}(s)}{v_{\rm MPPT}(s)} = \frac{1}{1 + \tau_f \cdot s}. \tag{30}$$

However, using a second-order filter, it is possible to obtain the same performance with a shorter settling time, which is desirable to enable shorter T_a values to improve the MPPT tracking speed. Therefore, this paper adopts the second-order filter given in (31), which considers a damping ratio $\zeta = 1$ to avoid overshoots in the reference of the SMC. In addition, this filter exhibits a settling time equal to $t_{s,2\rm nd} = \frac{5.8339}{W_n}$

$$\frac{v_{\rm ref}(s)}{v_{\rm MPPT}(s)} = \frac{W_n^2}{s^2 + 2 \cdot W_n \cdot s + W_n^2}. \tag{31}$$

The time response $Y_{\rm Fil}(t)$ of the second-order filter to a step input of magnitude $\Delta v_{\rm MPPT}$ is presented in (32), where W_n must be designed to guarantee that the SMC reference $v_{\rm ref}$ fulfills the constraints in (21) and (22). Such a design requires to evaluate both upper and lower limits within the operation range of the PV system, e.g., minimum and maximum PV voltages, to obtain the most restrictive limit for $\frac{dv_{\rm ref}}{dt}$, i.e., $\max\left(\frac{dv_{\rm ref}}{dt}\right)$

$$Y_{\rm Fil}(t) = \Delta v_{\rm MPPT} \cdot \left(1 - e^{-W_n \cdot t} \cdot (1 + W_n \cdot t)\right). \tag{32}$$

Then, the maximum value of the filtered voltage derivative (33) must be equal to $\max\left(\frac{dv_{\rm ref}}{dt}\right)$. The value of t at which (33) presents the global maximum is $t = \frac{1}{W_n}$, then the filter parameter W_n must be calculated as in (34)

$$\frac{dY_{\rm Fil}}{dt} = \Delta v_{\rm MPPT} \cdot \left(W_n^2 \cdot t \cdot e^{-W_n \cdot t}\right) = \max\left(\frac{dv_{\rm ref}}{dt}\right) \tag{33}$$

$$W_n = \frac{\max\left(\frac{dv_{\rm ref}}{dt}\right) \cdot e^1}{\Delta v_{\rm MPPT}}. \tag{34}$$

To illustrate the improvement of the system performance by using the second-order filter, the first-order filter in (30) was designed as proposed in [20]: $\tau_f = \frac{\Delta v_{\rm MPPT}}{\max\left(\frac{dv_{\rm ref}}{dt}\right)}$. Then, to obtain the same limitation $\max\left(\frac{dv_{\rm ref}}{dt}\right)$ in the dynamic behavior of the SMC reference, the second-order filter provides a settling time 54% shorter than the first-order option. Hence, taking into account that $T_a \geq t_s$ [19], the second-order filter enables to implement a faster P&O algorithm.

D. Calculation of K_1 and W_n

The effect of the reference filter in the settling time of the complete system must be considered. Otherwise, the settling time of the PV voltage will not be the desired one, which makes impossible to guarantee $T_a \geq t_s$. In addition, the PV voltage could exhibit overshoots that degrade the power generation. This is the case of the design process given in [20], which does not take into account the filter effect into the PV voltage dynamics.

In contrast, parameter K_1 in this paper is designed to achieve a desired settling time t_s of the PV voltage imposed by the P&O algorithm: The complete time response of the PV system composed of both (18) and (31) is given in (35), shown at the bottom of the next page, where the value of K_1 depends on the desired $t = t_s \leq T_a$ and $\Delta v_{\rm MPPT}$

$$\lim_{\Psi \to 0^-} \frac{d\Psi}{dt} = \frac{v_{\rm PV}}{dt} \cdot (K_1 + K_2 \cdot Y) - K_1 \cdot \frac{dv_{\rm ref}}{dt} + K_2 \cdot \frac{di_{\rm SC}}{dt} - K_2 \cdot \left(\frac{v_{\rm PV}}{L}\right) > 0 \tag{25}$$

$$\lim_{\Psi \to 0^+} \frac{d\Psi}{dt} = \frac{v_{\rm PV}}{dt} \cdot (K_1 + K_2 \cdot Y) - K_1 \cdot \frac{dv_{\rm ref}}{dt} + K_2 \cdot \frac{di_{\rm SC}}{dt} - K_2 \cdot \left(\frac{v_{\rm PV} - v_b}{L}\right) < 0 \tag{26}$$

E. Summary of the Design Procedure

The design of the SMC is based on the requirements of the P&O algorithm used to perform the MPPT: Perturbation magnitude Δv_{MPPT} and period T_a. Moreover, practical constraints must be also considered, e.g., maximum switching frequency, maximum inductor current ripple, voltage constraints of the circuits implementing the hysteresis band, etc.

The first step is to define $\Delta i_{C_{\mathrm{in}}}$ from requirements on Δi_L, PV voltage ripple, or switching frequency (28). Then, K_2 is designed from (29) based on the desired hysteresis band H and $\Delta i_{C_{\mathrm{in}}}$ value. Subsequently, constraints in (21) and (22) must be evaluated within the operation range of the PV system, where the maximum reference derivative $\max\left(\frac{dv_{\mathrm{ref}}}{dt}\right)$ permissible depends on the parameter K_1. These expressions together with (34) and (35) form a nonlinear equation system that must be solved by means of numerical methods, e.g., Newton–Raphson, Trust-Region, Levenberg–Marquardt, genetic algorithms, among others. The solution of the equation system gives the required values of K_1 and W_n to guarantee the SMC desired behavior.

V. Simulation Results

The proposed procedure to analyze and design the SMC for the PV system in Fig. 5 is illustrated in the following conditions. An irradiance operation range within $100\ \mathrm{W/m^2} \leq S \leq 1000\ \mathrm{W/m^2}$ with a maximum continuous irradiance derivative $\frac{dS}{dt} = 1\ \mathrm{kW/\left(m^2 \cdot s\right)}$, which simulates a transition from the highest irradiance to complete shade in 1 s. The adopted PV module is a BP585 with average parameters $i_{\mathrm{SC}} = 5$ A, $I_R = 11.6$ nA, $\alpha = 0.9009\ \mathrm{V^{-1}}$, $K_S = 0.005\ \left(\mathrm{A \cdot m^2}\right)/\mathrm{W}$, and MPP voltages between 16.39 and 18.13 V. The parameters of the dc/dc converter are $L = 22.5\ \mu$H, $C_{\mathrm{in}} = 66\ \mu$F, $C_o = 66\ \mu$F, $v_b = 29$ V, and a PV voltage operation within $10\ \mathrm{V} \leq v_{\mathrm{PV}} \leq 20\ \mathrm{V}$. In addition, the load perturbations generated by a grid-connected inverter consider a grid frequency $f_{\mathrm{grid}} = 50$ Hz and a maximum variation of v_b equal to 34.5%, i.e., $24\ \mathrm{V} \leq v_b \leq 34\ \mathrm{V}$.

The SMC design considers the following P&O parameters: $T_a = 2$ ms and $\Delta v_{\mathrm{MPPT}} = 2$ V. To ensure the P&O stability, the desired settling time of the PV voltage is set to $t_s = 0.5$ ms, but many other $t_s \leq T_a$ can be adopted. Concerning practical limitations, the switching frequency must be smaller than 95 kHz, and the implementation of the control action in Fig. 6 is performed using a TS555 integrated circuit, which imposes an hysteresis band $H = 1.667$ V for a supply voltage $V_{cc} = 5$ V.

The current ripple of the input capacitor is calculated from (28) at the maximum load voltage and MPP voltage obtaining $\Delta i_{C_{\mathrm{in}}} = 4$ A. Then, the magnitude of K_2 is calculated from (29), obtaining $K_2 = -0.417\ \mathrm{V/A}$.

Subsequently, the equations system formed by (21), (22), (34), and (35) is solved using the $f$solve() function of MATLAB with the Trust-Region method, obtaining $K_1 = -0.212$ and $W_n = 1.0535 \times 10^6\ \mathrm{rad/s}$ with a maximum derivative of the reference $\max\left(\frac{dv_{\mathrm{ref}}}{dt}\right) = 0.76\ \mathrm{V}/\mu\mathrm{s}$.

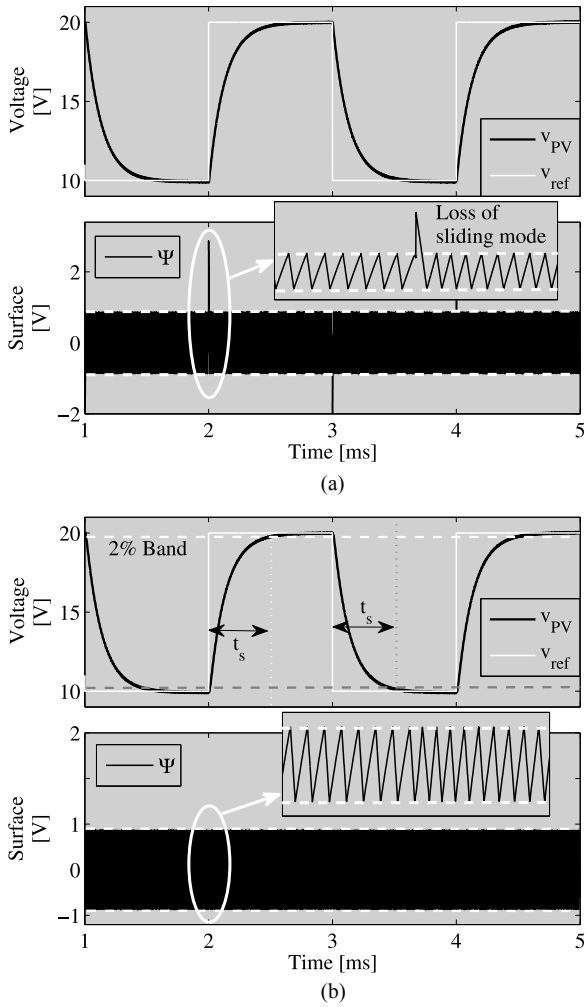

Fig. 7. Simulation of the SMC. (a) Without the filter [see Fig. 4(a)]. (b) With the filter (see Fig. 5).

Despite the SMC was designed for a continuous irradiance derivative $\frac{dS}{dt} = 1\ \mathrm{kW/\left(m^2 \cdot s\right)}$ in dynamic conditions of the reference, when the system is in steady state, e.g., with constant reference, the SMC is able to support much faster irradiance changes. Such a condition is evaluated from (19) and (20) by replacing $\frac{dv_{\mathrm{ref}}}{dt} = 0$ to obtain $-80.36\ \mathrm{MW/\left(m^2 \cdot s\right)} < \frac{dS}{dt} < 90.51\ \mathrm{MW/\left(m^2 \cdot s\right)}$, which correspond to near step irradiance transitions.

Fig. 7 presents the simulation of the SMC for step-like up and down variations in the reference of 10 V. The simulation in Fig. 7(a) corresponds to the scheme in Fig. 4(a), which does not include the filter: Despite the SMC forces the PV voltage

$$\left.\begin{aligned} v_{\mathrm{PV}}(t) &= \left(1 + a \cdot e^{-W_n \cdot t} + b \cdot t \cdot e^{-W_n \cdot t} - c \cdot e^{\frac{-t}{Q}}\right) \cdot \Delta v_{\mathrm{MPPT}}\Big|_{t=t_s} \\ Q &= \tfrac{K2 \cdot C_{\mathrm{in}}}{K_1}, \quad a = \tfrac{2 \cdot W_n \cdot Q - 1}{(W_n \cdot Q - 1)^2}, \quad b = \tfrac{W_n}{W_n \cdot Q - 1}, \quad c = \tfrac{W_n^2 \cdot Q^2}{(W_n \cdot Q - 1)^2} \end{aligned}\right\} \tag{35}$$

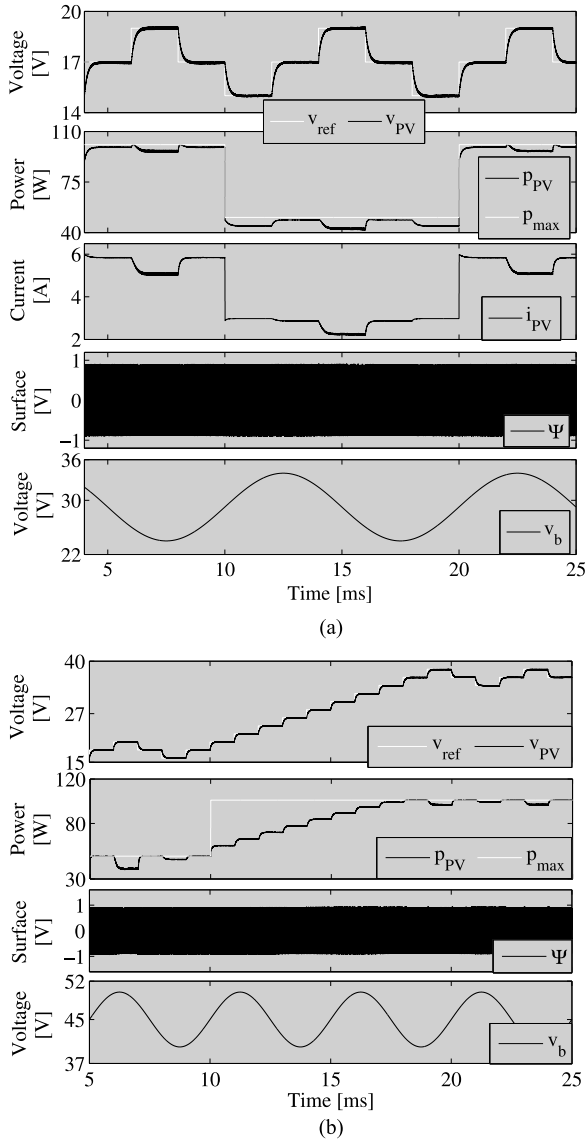

Fig. 8. Simulation of the PV system with perturbations in the bulk voltage. (a) For changes in the irradiance. (b) For changes in the PV operation voltage.

to satisfactorily track the reference $v_{\rm ref}$, the sliding mode is lost at the instant the reference changes. Such a condition validates the requirement of constraining the derivative of the reference described in (21) and (22). In contrast, Fig. 7(b) presents the simulation of the scheme in Fig. 5, which includes the filter: The SMC ensures the tracking of the reference while the surface operates into the hysteresis band for all the conditions, i.e., the sliding mode holds even in the step-like transients of $v_{\rm ref}$. Moreover, the characteristics of the PV voltage confirm the accurate calculation of parameters K_1, K_2, and W_n: A null overshoot and a settling time $t_s = 0.5$ ms, both matching the design requirements.

Fig. 8(a) presents a simulation of the PV system with the voltage reference provided by the P&O algorithm. Moreover, the simulation considers 100 Hz voltage oscillations in the load voltage v_b to illustrate the satisfactory mitigation of bulk voltage perturbations. This simulation shows a correct tracking of the P&O reference with the desired setting time $t_s = 0.5$ ms in presence of large load voltage variations of 34.5%. The correct operation of the P&O is confirmed by the accurate tracking of the maximum PV power available $p_{\rm max}$. The simulation considers a PV array formed by two BP585 panels in parallel, both with an irradiance level of $S = 600$ W/m^2. At $t = 10$ ms, one of the panels is disconnected to simulate a step-like disturbance of 50% in PV current, and at $t = 20$ ms, the PV module is connected again. The results show the accurate tracking of the MPP and the satisfactory mitigation of the perturbations, which demonstrates the effectiveness of the proposed design procedure.

Fig. 8(b) presents a similar simulation but considering a PV array formed by two BP585 panels in series. The PV system operates with a single panel up to $t = 10$ ms, from that instant, the second panel is connected to illustrate the tracking performance when the optimal PV voltage changes considerably. Again, the designed SMC enables the P&O to track the new MPP.

To illustrate the improvement of the proposed design method over the procedures reported in [15] and [20], the design of the SMC based on Ψ in (6) is contrasted with the design of the controller based on Ψ_{i_L} in (1), reported in [15], and with the design of the controller based on $\Psi_{i_{C_{\rm in}}}$ in (3), reported in [20]. To perform a fair comparison, the linear controllers required for both Ψ_{i_L} and $\Psi_{i_{C_{\rm in}}}$ were designed to provide null overshoot and a settling time equal to 0.5 ms. Fig. 9(a) presents the controllers response to a step change in the reference, where both Ψ_{i_L} and $\Psi_{i_{C_{\rm in}}}$ options do not fulfill the overshoot and settling time requirements.

To provide comparisons in different operating conditions, the three controllers were redesigned for 19 different settling times between 0.1 and 1.0 ms. Fig. 9(b)–(d) compares the settling time errors, overshoots, and energy losses provided by the three options. Those simulations confirm that the design procedure proposed in this paper ensures the required settling time and overshoot, while the design procedures reported in [15] and [20] lead to large errors in both the settling time and overshoot as analyzed in Sections II and III.

Moreover, the inaccurately long settling times provided by both $\Psi_{i_{C_{\rm in}}}$ and Ψ_{i_L}, e.g., 350% to 450% in some cases, could lead to violate the P&O stability condition $T_a \geq t_s$. In addition, the longer settling times and overshoots make both $\Psi_{i_{C_{\rm in}}}$ and Ψ_{i_L} produce larger energy losses, 30% to 45% in some cases.

The simulations presented in this section put in evidence the effectiveness of the proposed design procedure, since the SMC based on Ψ provides a correct tracking of MPP, in presence of perturbations in both irradiance level and load voltage, for a wide operation range. Moreover, the simulations also confirm the advantages of the proposed procedure over the design methods reported in [15] and [20].

VI. Implementation and Experimental Results

This section presents experimental validations of the proposed design procedure. The experimental test bench consists in a PV array made of two BP585 modules, a boost dc/dc converter, an electronic load, a DSP device with a MCP4822 digital-to-analog converter (DAC) to implement the P&O as in

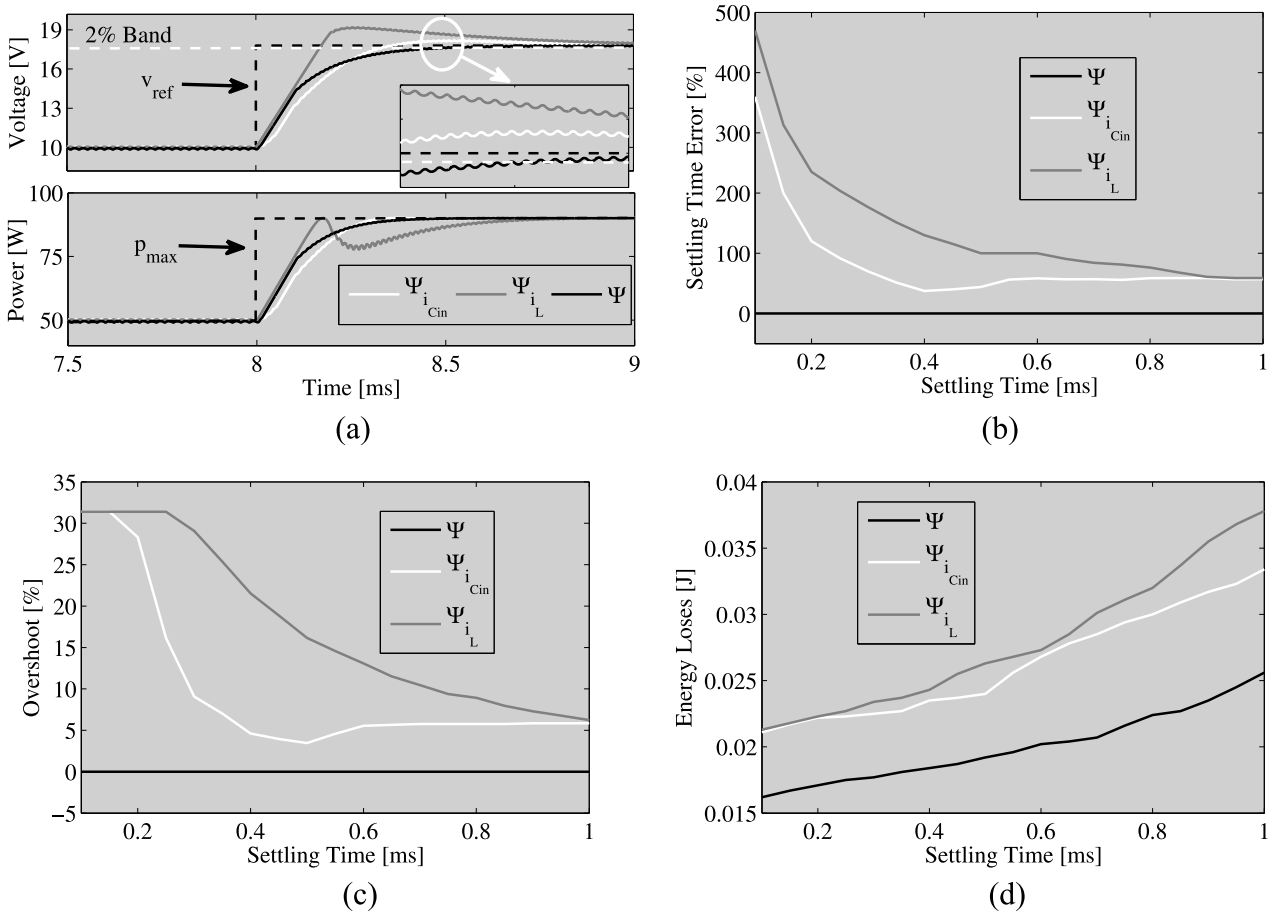

Fig. 9. Performance comparison of the SMC based on Ψ, Ψ_{i_L} [15], and $\Psi_{i_{C_{\rm in}}}$ [20] designed for different settling times. (a) Time responses for $t_s = 0{:}5$ ms. (b) Settling time error. (c) Overshot. (d) Energy losses.

[7], and a circuit based on operational amplifiers and a TS555 to implement the SMC. The TS555 and all OpAmps (rail-to-rail TLC2272 and OPA2350) are unipolar 5-V powered. The structure of the experimental platform is presented in Fig. 10, where the PV panels can be connected in series or parallel depending on the test. Additional switches make possible the connection or disconnection of the PV modules to emulate 50% step-like irradiance transients or to instantaneously change the optimal PV voltage. The converter, PV array, settling time, and P&O parameters are the same ones that are previously adopted for the simulation results; therefore, the SMC parameters K_1, K_2, and W_n calculated in Section V hold for the experimental system. The laboratory setup is presented in Fig. 11, which also shows the PC used to program the DSP.

The reference filter in Fig. 10 was implemented using analog components, i.e., two resistors and two capacitors. However, since a DSP is used to process the P&O algorithm, it is possible to discretize such a filter to be processed by the DSP.

The DAC used in the experimental platform has a minimum sampling time of $ts_F = 4.5$ μs, hence the digital filter must be designed accordingly: Fig. 12(a) shows the dynamic response of both the analog filter and its digital version with $ts_F = 4.5$ μs, where the digital filter exhibits a settling time 244% longer than the required one and an unacceptable overshoot. Therefore, using the MCP4822 DAC, it is not possible to implement a digital version of the reference filter. Fig. 12(a) also shows the performance of two digital filters designed with shorter sampling times $ts_F = 1.5$ μs and $ts_F = 0.5$ μs, where only the one with $ts_F = 0.5$ μs achieves the desired settling time (0.5 ms), but it requires a DAC nine times faster, i.e., a much costly device.

Another option is to implement a derivative limiter instead of a traditional filter. In this case, the step-like reference provided by the P&O becomes a ramp waveform with slope equal to $\max\left(\frac{dv_{\rm ref}}{dt}\right)$, where the time required by the ramp to reach the reference voltage is $t_{\rm RAMP} = \Delta v_{\rm MPPT} / \max\left(\frac{dv_{\rm ref}}{dt}\right)$. Then, the number of steps forming the digital ramp is $N_{\rm RAMP} = 1 + t_{\rm RAMP}/ts_F$. Using the DAC with $ts_F = 4.5$ μs adopted in the experimental platform $N_{\rm RAMP} = 1$, hence no slope limitation is performed as depicted in the simulations of Fig. 12(b). Such a figure also presents the digital ramps achieved with shorter $ts_F = 1.5$ μs and $ts_F = 0.5$ μs, where the first one provides two steps, while the latter one provides six steps. Again, a much faster DAC is needed, in comparison with the MCP4822, to achieve an acceptable digital ramp.

The previous analyses show that the adopted DAC forces the analog implementation of the reference filter. However, faster DACs enable to integrate the reference slope limitation into the digital device used to process the MPPT algorithm.

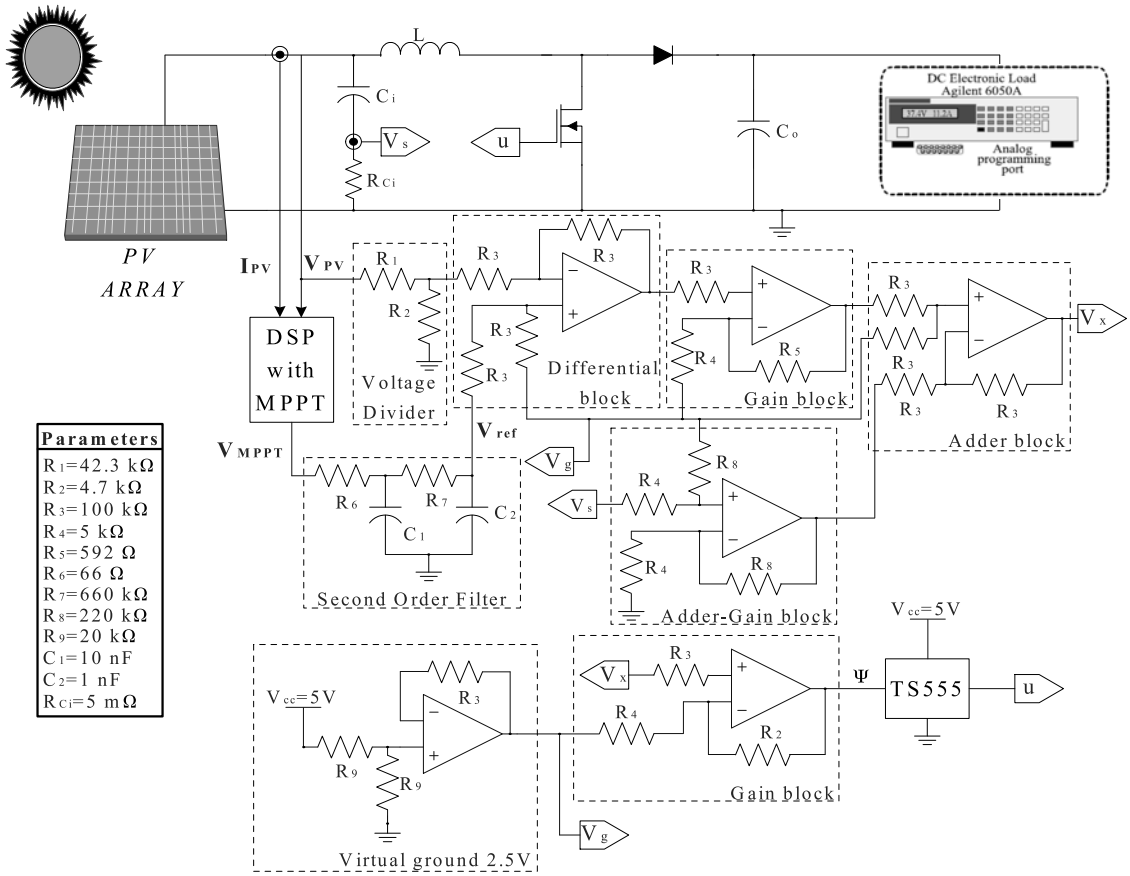

Fig. 10. Electrical scheme of the experimental test bench.

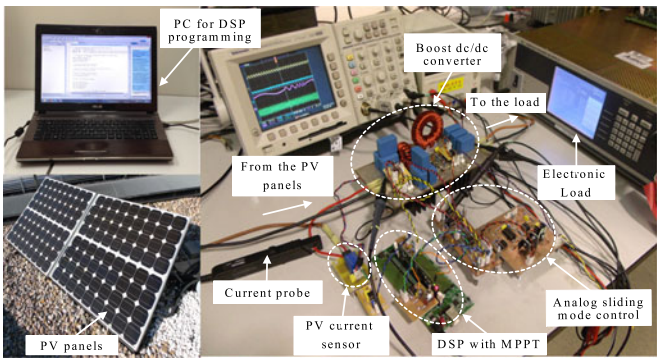

Fig. 11. Laboratory setup.

The proposed procedure for designing the SMC was validated by reproducing the simulation tests using the experimental platform of Fig. 10; Fig. 13 shows the experimental behavior of the PV system in presence of step commands injected to the reference, similar to the simulations presented in Fig. 7. This test validates the design of the analog filter added to the reference of the SMC to ensure the system operation inside the sliding band. Moreover, Fig. 13(b) validates the procedure to calculate K_1, K_2, and W_n to impose a desired settling time to the PV voltage including the filter effect.

Two additional experiments were made to verify the performance of the complete PV system including the MPPT algorithm: The first one considers a fast change in the irradiance, and the second one considers a fast change in the MPP voltage. In both tests, the electronic load was configured to impose a 100 Hz oscillation at the output port of the dc/dc converter to emulate a disturbance of 34.5% generated by a grid-connected inverter.

In the first case, the PV array is formed by two parallel connected modules. Then, one of those modules is disconnected to emulate a step-like 50% perturbation in the irradiance. Fig. 14(a) presents the experimental waveforms, where the P&O exhibits a stable three-point profile in presence of both the irradiance and load voltage perturbations, which put in evidence the satisfactory performance of the proposed design procedure. This experiment confirms the simulations reported in Fig. 8(a).

In the second case, the PV array is originally formed by a single module. Then, an additional module is connected in series to produce a fast change on the MPP voltage. Fig. 14(b) presents the results of this experiment, where the P&O accurately tracks the new MPP in presence of the load voltage perturbations, which verifies again the satisfactory performance of the design procedure. This experiment confirms the simulations reported in Fig. 8(b).

Finally, the experimental results presented in this section validate the correctness of the proposed procedure to design

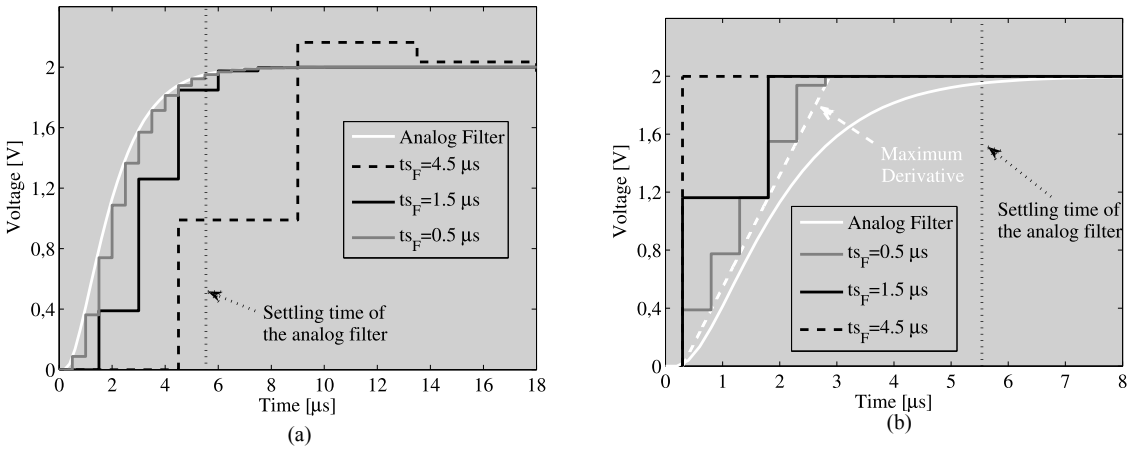

Fig. 12. Digital implementations of the reference filter. (a) Digital filter. (b) Digital derivative limitation.

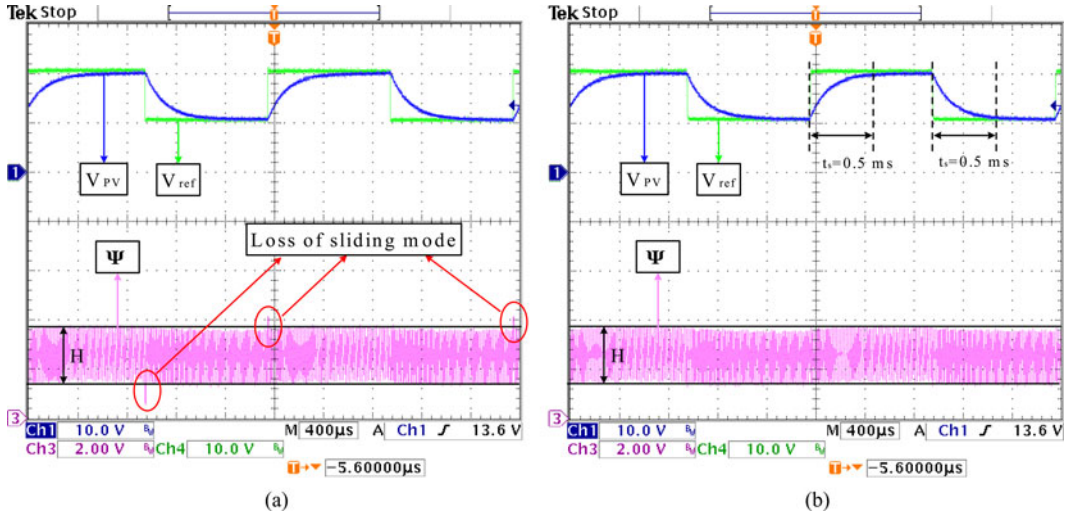

Fig. 13. Experimental verification of the SMC performance. (a) Without filter. (b) With filter.

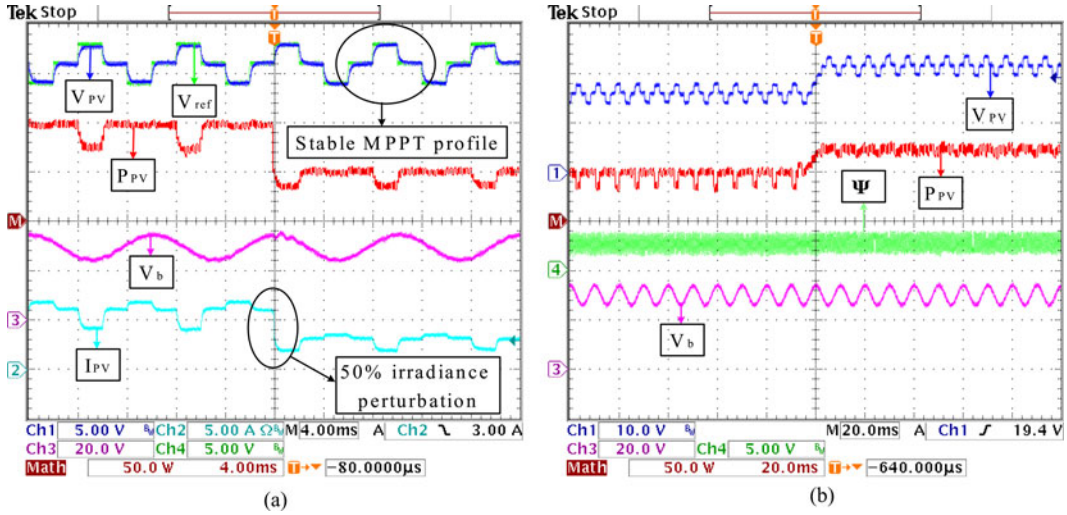

Fig. 14. Experimental verification of the PV system performance. (a) For changes on the irradiance. (b) For changes of the MPP voltage.

the SMC in agreement with the requirements of the MPPT algorithm.

VII. Conclusion

This paper has proposed an improved procedure for designing the SMC of a boost converter in a grid-connected PV system. Its PV voltage tracked the reference provided by an external MPPT with a specified settling time and no overshoot while being insensitive to changes in environmental conditions, such as solar irradiation or PV module temperature, and the 100/120-Hz perturbations in the bulk capacitor voltage linking the boost converter and the cascaded inverter connected to the grid. In the analysis of the selected switching surface, formed by a linear combination of the input capacitor current and the PV voltage error, a single control loop has been considered. This approach differs from other similar solutions previously reported that used cascade controllers based on inner fast current control loops and outer voltage loops designed after a linearization of the current loop dynamic response. Avoiding the linearization, it is a key feature of the improved procedure because the validity of the analytical expressions is not restricted around an operating point, provided that the sliding regime is not lost.

As expected from other solutions, the expression of the equivalent control obtained in the sliding analysis indicated that a low-pass prefilter had to be inserted between the MPPT module and the controller input, so that the usually large time derivatives in the MPPT-provided reference voltage were sufficiently limited to avoid losing the sliding regime. It has been found that instead of the first-order low-pass filter of previous solutions, a second-order critically damped filter provided the same smoothing functionality but with much shorter settling times. While the poorly designed filters of previous approaches caused the controllers to fail in providing the PV voltage responses with no overshoot and the specified settling times required by MPPT, simulation and experimental results showed that the controller is designed following the improved procedure fulfilled correctly all these requirements. The controller parameters were calculated by solving a nonlinear set of equations obtained by combining the filter design equations with the restrictions necessary for the sliding regime to hold in all the PV module and dc/dc converter operating points.

In the simulations and experiments, a SMC with a very simple variable switching frequency hysteretic modulation was considered. A description of the experimental setup together with a detailed controller implementation based in rail-to-rail OpAmps and the well-known 555 timer, powered by a 5-V unipolar supply, has been provided to help readers in reproducing the experimental results.

Finally, the same detailed analysis and design of SMC can be applied in further developments to PV systems based on other converter topologies such as buck (e.g., battery charges), buck–boost (e.g., module optimizers), inverters (e.g., PV microinverters), among others.

References

[1] E. Koutroulis, K. Kalaitzakis, and N. Voulgaris, "Development of a microcontroller-based, photovoltaic maximum power point tracking control system," *IEEE Trans. Power Electron.*, vol. 16, no. 1, pp. 46–54, Jan. 2001.

[2] B. Yang, W. Li, Y. Zhao, and X. He, "Design and analysis of a grid-connected photovoltaic power system," *IEEE Trans. Power Electron.*, vol. 25, no. 4, pp. 992–1000, Apr. 2010.

[3] R. Khanna, Q. Zhang, W. Stanchina, G. Reed, and Z.-H. Mao, "Maximum power point tracking using model reference adaptive control," *IEEE Trans. Power Electron.*, vol. 29, no. 3, pp. 1490–1499, Mar. 2014.

[4] N. Femia, G. Petrone, G. Spagnuolo, and M. Vitelli, "Optimization of perturb and observe maximum power point tracking method," *IEEE Trans. Power Electron.*, vol. 20, no. 4, pp. 963–973, Jul. 2005.

[5] C. Konstantopoulos and E. Koutroulis, "Global maximum power point tracking of flexible photovoltaic modules," *IEEE Trans. Power Electron.*, vol. 29, no. 6, pp. 2817–2828, Jun. 2014.

[6] T. Esram, J. Kimball, P. Krein, P. Chapman, and P. Midya, "Dynamic maximum power point tracking of photovoltaic arrays using ripple correlation control," *IEEE Trans. Power Electron.*, vol. 21, no. 5, pp. 1282–1291, Sep. 2006.

[7] R. Mastromauro, M. Liserre, and A. Dell'Aquila, "Control issues in single-stage photovoltaic systems: MPPT, current and voltage control," *IEEE Trans. Ind. Informat.*, vol. 8, no. 2, pp. 241–254, May 2012.

[8] T. Esram and P. L. Chapman, "Comparison of photovoltaic array maximum power point tracking techniques," *IEEE Trans. Energy Convers.*, vol. 22, no. 2, pp. 439–449, Jun. 2007.

[9] N. Femia, G. Petrone, G. Spagnuolo, and M. Vitelli, "A new analog MPPT technique: Teodi," *Prog. Photovoltaics, Res. Appl.*, vol. 18, no. 1, pp. 28–41, 2010.

[10] G. Walker and P. Sernia, "Cascaded dc-dc converter connection of photovoltaic modules," *IEEE Trans. Power Electron.*, vol. 19, no. 4, pp. 1130–1139, Jul. 2004.

[11] G. Petrone, G. Spagnuolo, R. Teodorescu, M. Veerachary, and M. Vitelli, "Reliability issues in photovoltaic power processing systems," *IEEE Trans. Ind. Electron.*, vol. 55, no. 7, pp. 2569–2580, Jul. 2008.

[12] A. Trejos, D. Gonzalez, and C. A. Ramos-Paja, "Modeling of step-up grid-connected photovoltaic systems for control purposes," *Energies*, vol. 5, no. 6, pp. 1900–1926, 2012.

[13] J. Chavarria, D. Biel, F. Guinjoan, C. Meza, and J. Negroni, "Energy-balance control of PV cascaded multilevel grid-connected inverters under level-shifted and phase-shifted PWMs," *IEEE Trans. Ind. Electron.*, vol. 60, no. 1, pp. 98–111, Jan. 2013.

[14] S.-C. Tan, Y. M. Lai, and C. K. Tse, "General design issues of sliding-mode controllers in dc-dc converters," *IEEE Trans. Ind. Electron.*, vol. 55, no. 3, pp. 1160–1174, Mar. 2008.

[15] E. Bianconi, J. Calvente, R. Giral, E. Mamarelis, G. Petrone, C. A. Ramos-Paja, G. Spagnuolo, and M. Vitelli, "Perturb and observe MPPT algorithm with a current controller based on the sliding mode," *Int. J. Electr. Power Energy Syst.*, vol. 44, no. 1, pp. 346–356, 2013.

[16] J. Knight, S. Shirsavar, and W. Holderbaum, "An improved reliability cuk based solar inverter with sliding mode control," *IEEE Trans. Power Electron.*, vol. 21, no. 4, pp. 1107–1115, Jul. 2006.

[17] E. Mamarelis, G. Petrone, and G. Spagnuolo, "Design of a sliding-mode-controlled SEPIC for PV MPPT applications," *IEEE Trans. Ind. Electron.*, vol. 61, no. 7, pp. 3387–3398, Jul. 2014.

[18] Y. Levron and D. Shmilovitz, "Maximum power point tracking employing sliding mode control," *IEEE Trans. Circuits Syst. I, Reg. Papers*, vol. 60, no. 3, pp. 724–732, Mar. 2013.

[19] N. Femia, G. Petrone, G. Spagnuolo, and M. Vitelli, "A technique for improving P&O MPPT performances of double-stage grid-connected photovoltaic systems," *IEEE Trans. Ind. Electron.*, vol. 56, no. 11, pp. 4473–4482, Nov. 2009.

[20] E. Bianconi, J. Calvente, R. Giral, E. Mamarelis, G. Petrone, C. A. Ramos-Paja, G. Spagnuolo, and M. Vitelli, "A fast current-based MPPT technique employing sliding mode control," *IEEE Trans. Ind. Electron.*, vol. 60, no. 3, pp. 1168–1178, Mar. 2013.

[21] Q. Li and P. Wolfs, "A review of the single phase photovoltaic module integrated converter topologies with three different dc link configurations," *IEEE Trans. Power Electron.*, vol. 23, no. 3, pp. 1320–1333, May 2008.

[22] G. Petrone and C. Ramos-Paja, "Modeling of photovoltaic fields in mismatched conditions for energy yield evaluations," *Electr. Power Syst. Res.*, vol. 81, no. 4, pp. 1003–1013, 2011.

[23] U. Eicker, *Solar Technologies for Buildings*. New York, NY, USA: Wiley, 2003.

[24] H. Sira-Ramirez, "Sliding motions in bilinear switched networks," *IEEE Trans. Circuits Syst.*, vol. CAS-34, no. 8, pp. 919–933, Aug. 1987.

[25] R. Erickson and D. Maksimovic, *Fundamentals of Power Electronics*. New York, NY, USA: Kluwer, 2004.

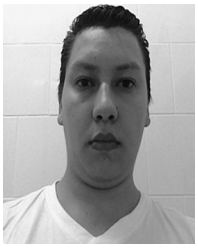

Daniel González Montoya received the Engineering degree in control and the Masters' degree in industrial automatic from the Universidad Nacional de Colombia, Manizales, Columbia, in 2010 and 2012, respectively, and is currently working toward the Ph.D. degree in automatic engineering from the same university.

His main research interests include the design control strategies of renewable energy systems and switching converters.

Carlos Andrés Ramos-Paja was born in Cali, Colombia, in 1978. He received the Engineering degree in electronics and the Masters' degree in automatic control from the Universidad del Valle, Cali, in 2003 and 2005, respectively, and the Ph.D. degree in power electronics from the Universitat Rovira i Virgili, Tarragona, Spain, in 2009.

Since 2009, he has been a Professor in the Universidad Nacional de Colombia, Manizales, Columbia, where since 2012, he is an Associate Professor. His main research interests include the design and control of renewable energy systems, switching converters, distributed power systems, and power quality solutions.

Roberto Giral (S'94–M'02–SM'10) received the B.S. degree in ingeniera tcnica de telecomunicacin, the M.S. degree in ingeniera de telecomunicacin, and the Ph.D. (with Hons.) degree from the Universitat Politcnica de Catalunya, Barcelona, Spain, in 1991, 1994, and 1999, respectively.

He is currently an Associate Professor with the Departament dEnginyeria Electrnica, Elctrica i Automtica, Escola Tcnica Superior dEnginyeria, Universitat Rovira i Virgili, Tarragona, Spain, where he is working in the field of power electronics.